

This is an Open Access document downloaded from ORCA, Cardiff University's institutional repository:<https://orca.cardiff.ac.uk/id/eprint/130308/>

This is the author's version of a work that was submitted to / accepted for publication.

Citation for final published version:

Meinke, J., Mauskopf, P., Johnson, B. R., Flanigan, D., Irwin, K., Li, D., Cho, H.-M., Day, P., McMahon, J., Doyle, S. and Ade, P. A. R. 2020. Planar self-similar antennas for broadband millimeter-wave measurements. *Journal of Low Temperature Physics* 199 , pp. 281-288. 10.1007/s10909-020-02427-0

Publishers page: <http://dx.doi.org/10.1007/s10909-020-02427-0>

Please note:

Changes made as a result of publishing processes such as copy-editing, formatting and page numbers may not be reflected in this version. For the definitive version of this publication, please refer to the published source. You are advised to consult the publisher's version if you wish to cite this paper.

This version is being made available in accordance with publisher policies. See <http://orca.cf.ac.uk/policies.html> for usage policies. Copyright and moral rights for publications made available in ORCA are retained by the copyright holders.



# Planar Self-Similar Antennas for Broadband Millimeter-Wave Measurements

J. Meinke<sup>1</sup> · P. Mauskopf<sup>1,2</sup> · B. R. Johnson<sup>3</sup> · D. Flanigan<sup>3</sup> · K. Irwin<sup>4</sup> · D. Li<sup>5</sup> · H.-M. Cho<sup>5</sup> · P. Day<sup>6</sup> · J. McMahon<sup>7</sup> · S. Doyle<sup>8</sup> · P. A. R. Ade<sup>8</sup>

the date of receipt and acceptance should be inserted later

**Abstract** Self-similar antennas offer extremely broadband functionality and easily scalable designs. Self-similar designs with a four-arm layout are also suited for dual-polarization through excitations of opposing arms, although there has only been limited use of them for millimeter-wave detectors. These antennas have been used for measurements of the Cosmic Microwave Background (CMB), which encompass a wide frequency range and are now actively focusing more on polarization anisotropies. We analyze multiple planar self-similar antenna designs with simulations in HFSS (High Frequency Structure Simulator) and ongoing physical testing. They all exhibit broadband operation between 130-230 GHz and can couple to both linear polarizations through the previously mentioned four-arm symmetry. Simulations include each antenna design coupled to an extended hemispherical, AR-coated lenslet. From these, a basic bowtie-like arm design produced minimal polarization wobble with moderate beam efficiency, while a hybrid trapezoidal design provided high beam efficiency with small polarization wobble. Current fabrication versions of each are being tested, coupled to multichroic Microwave Kinetic Inductance Detectors (MKIDs). These planar self-similar antennas, when implemented in CMB and other detectors, could improve observations while simultaneously simplifying fabrication and detector layout.

**Keywords** Antennas, Kinetic Inductance Detector (KID), CMB, Polarization

## 1 Introduction

The concept of self-similar and self-complementary antennas for wide bandwidth applications has been around for decades, primarily investigated at radio frequencies. Popular designs used today include the log-periodic radio antenna with dipole-like rods scaled logarithmically, and various spiral planar or conical antennas [1]. The main focus of these

---

<sup>1</sup> Department of Physics, Arizona State University, Tempe, Arizona 85287, USA

<sup>2</sup> School of Earth and Space Exploration, Arizona State University, Tempe, Arizona 85287, USA

<sup>3</sup> Department of Physics, Columbia University, New York, NY 10027, USA

<sup>4</sup> Department of Physics, Stanford University, Stanford, CA 94305-4085, USA

<sup>5</sup> SLAC National Accelerator Laboratory, Menlo Park, CA 94025, USA

<sup>6</sup> NASA, Jet Propulsion Lab, Pasadena, CA 91109, USA

<sup>7</sup> Department of Physics, University of Michigan, Ann Arbor, MI 48103, USA

<sup>8</sup> School of Physics and Astronomy, Cardiff University, Cardiff CF243AA, UK

devices was the potential versatility of a broadband antenna applicable for more compact and efficient communication. Many also cite self-complementary antennas as frequency-independent due to their scalability and arm impedance in an  $n$ -arm design that follows an altered Babinet's Principle, shown by Deschamps [2]:

$$Z_{slot}Z_{metal} = \left( \frac{Z_0}{4\sin(\frac{\pi}{n})} \right)^2 \quad (1)$$

Which can be simplified for self-complementary planar layouts, where the metal/conductor arms are identical to the slots between them ( $Z_{metal} = Z_{slot}$ ). For an  $n = 4$  arm pattern in free space ( $Z_0 = 120\pi$ ), the arm impedance is roughly  $133 \Omega$ .

A four-arm self-complementary design (such as Fig. 1 further below), with each identical arm rotated  $90^\circ$  from the previous, grants the ability for dual-polarization [3]. One pair of opposing arms couples to a single linear polarization, allowing the entire antenna to couple to orthogonal linear polarizations. Hence, such multi-terminal antennas are well-suited for broadband polarization measurements.

A notable application and goal of the designs in this paper is the Cosmic Microwave Background (CMB), which is most prevalent at millimeter wavelengths due to an observed black-body radiation temperature of 2.726 K. Ground-based CMB detector frequency bands are often centered in the mm-wave atmospheric windows near 95, 150, and 220 GHz [4, 5]. After successful full-sky CMB missions like the Wilkinson Microwave Anisotropy Probe (WMAP) and Planck satellite, and high-resolution temperature investigations with the South Pole Telescope (SPT), Atacama Cosmology Telescope (ACT) and many others, the CMB observational focus is now directed towards precise polarization measurements of the CMB E- and B-modes [6]. This article goes through the design of self-similar/complementary antennas coupled to extended hemisphere lenslets (Section 2) and their viability of use for CMB mm-wave polarimetry (Section 3), primarily analyzed via High Frequency Structure Simulations (HFSS). Future plans and physical testing are then briefly outlined (Section 4).

## 2 Antenna Designs

An ideal antenna for such CMB detection requires a constant matchable impedance for the frequency bands, and high beam efficiency (directivity in the main beam,  $> 50\%$  desired). Other parameters such as linear polarization wobble (change in polarization alignment at the zenith), maximum cross-polarization contamination (x-pol, % of directivity in the wrong polarization) and ellipticity, should be reduced as low as possible.

The premise of these self-similar antennas is rotational symmetry. As mentioned, a four-arm design places an identical arm every  $90^\circ$ , while the complementary property requires there to be an identical slot or gap between them. The most basic design is a dual-bowtie antenna (Fig. 1), with inner ( $r_i$ ) and outer ( $r_o$ ) arm radii scaled to operating wavelengths. The simplicity in geometry also grants uniform current density at constant radius, minimizing fluctuations in both impedance and polarization. The downsides that promote investigation into other designs include a weak beam efficiency and noticeable x-pol.

### 2.1 Logarithmic Periodic Designs

Log-periodic self-complementary designs are another class of promising planar antennas. The side of each arm is defined by a periodic unit cell pattern in radial log-space, oscillating

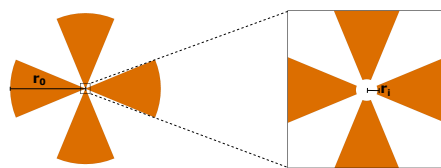


**Fig. 1** *Left*: A basic bowtie self-similar antenna layout, with the *orange* corresponding to the superconductor arms. The slots are identical in shape to the arms themselves, and the arms are not directly connected in the center (close-up, *right*). No scale bar is included as this antenna can be scaled invariantly according to frequency range. Simulation parameters used for this antenna type are in Section 3. (Color figure online)

between an angular amplitude of  $\pm\omega$ . Then the angular difference between arm sides is  $\delta$ , with a unit cell expansion rate of  $\tau$  that characterizes half the length of the unit cell (from [7]). For  $M$  unit cells and an inner radius  $r_i$ , the outer radius is defined as  $r_o = r_i \tau^{2M}$ .

An  $n = 4$  arm self-complementary layout requires  $\delta = \frac{360^\circ}{2n} = 45^\circ$ , while  $\tau > 1$  can vary. Common examples are the sinuous and trapezoidal unit cells with  $\omega = 45^\circ$  ( $\omega$  often chosen as this for better polarization), shown in Fig. 2 alongside their respective antenna patterns. The sinuous design has been extensively analyzed at mm-scales for similar CMB detection

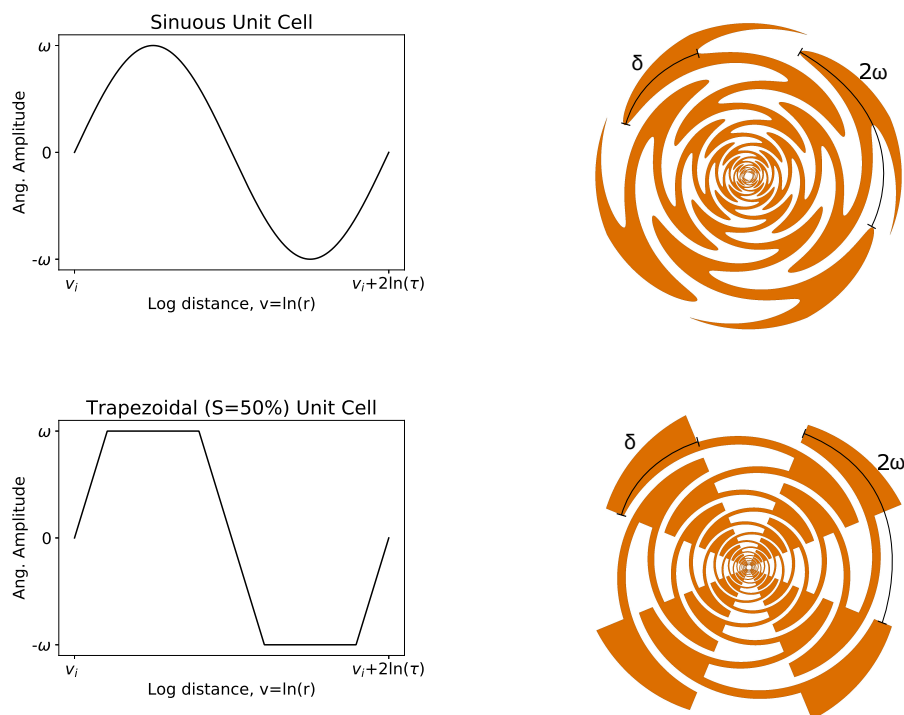


**Fig. 2** *Left*: Log-space unit cells for the Sinuous (*top*) and Trapezoidal (*bottom*) designs. Both respective antenna patterns (*right*) have  $n = 4$  arms with  $M = 7$  unit cells each. These can also be scaled invariantly. Note the trapezoidal design has an additional slope parameter  $S$ , that corresponds to the percentage of the unit cell at a max/min ( $\pm\omega$ ,  $S = 50$  shown).  $S = 100$  produces a rectangular unit cell, while  $S = 0$  is triangular. (Color figures online)

[4, 7, 8, 9], while the trapezoidal has mainly undergone testing at larger wavelengths [3, 10]. The trapezoidal design has an additional slope parameter  $0 \leq S < 100$  that designates the percentage the unit cell spends at a max/min ( $\pm\omega$ ). Polarization wobble was found to decrease as  $S \rightarrow 100$  (rectangular unit cell shape).

## 2.2 Lenslet Design

To optimize these antennas, an extended hemispherical silicon lenslet is placed over the antenna (Fig. 3, *left*). The high relative permittivity of silicon keeps the majority of the beam forward and shifts the central impedance of Eq. (1) down to  $52.5\Omega$ . To reduce reflection at the lens interface, a two-layer anti-reflection (AR) coating is applied [7, 9]. The addition of the lenslet reduces linear polarization wobble by focusing the main beam, but also amplifies frequency variations in impedance due to reflections at the silicon half-space.

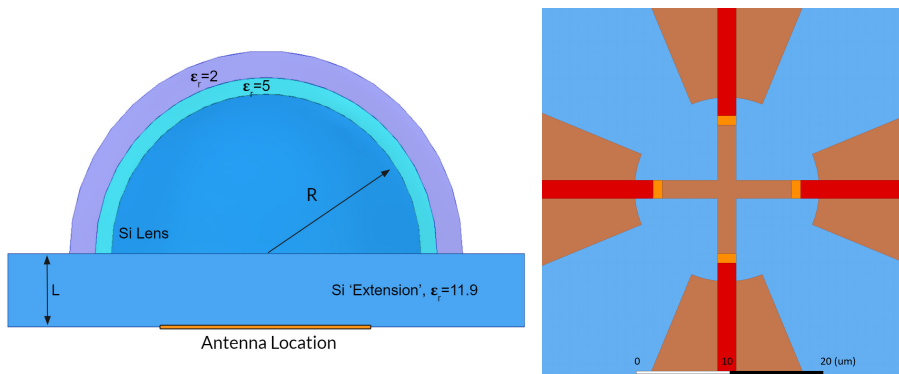


**Fig. 3** *Left*: Cross-section view of extended hemispherical lenslet to be coupled to antennas. The extension and lens are silicon ( $\epsilon_r = 11.9$ ), with two anti-reflection (AR) coatings over the lens to improve efficiency. Lens radius  $R$  scales with the antenna outer radius ( $r_o$ ) and highest  $\lambda/4$ . *Right*: Close-up view of bowtie antenna pattern with microstrips (*red*) over the arms, that connect down to a central cross feed, exciting the slot/gap between the center and the arm in the process. (Color figures online)

## 2.3 Central Feed

These broadband antennas need to be fed at the center in order for the lowest modes to be excited. When fabricated, the antenna designs are cut out of a ground plane, allowing a microstrip to be placed over each ground arm to the center. At inner arm radius  $r_i$  the microstrip passes over and excites a slot/gap between the ground arm and an independent plus-shaped cross feed in the ground plane, before connecting down to the cross feed as a virtual ground (Fig. 3, *right*). The orthogonal shape of the center minimizes cross-talk from perpendicular microstrips without the need for cross-overs [9]. From the self-complementary property, the excited slots function just as the arms would.

The use of microstrips for the trapezoidal design poses an additional issue though, as the narrower arm portions at low wavelengths become too small ( $< 2\mu\text{m}$ ) for an adequate microstrip to be run over them. This is especially the case for higher trapezoidal slope  $S$  values, which produced smaller polarization wobble.

## 2.4 Hybrid Trapezoidal Design

A solution around the just mentioned microstrip issue is to modify the trapezoidal design. The narrow widths can be held constant by changing the slope parameter  $S$  with radius (so  $S$  has the maximum allowed value at all radii for the desired microstrip). This removes the log-periodic classification, but maintains the self-complementary property. The hybrid trapezoidal designs were made to have a minimum width of  $4\mu\text{m}$  for a  $2\mu\text{m}$  wide microstrip plus padding on either side. This changes the first trapezoidal cell to look like Fig. 4 *left*, becoming more rectangular ( $S \rightarrow 100$ ) as radius increases.

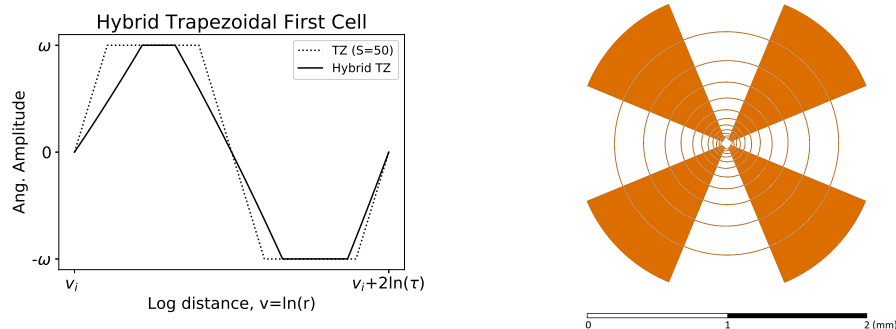


**Fig. 4** *Left*: First cell of the hybrid trapezoidal design (no longer log-periodic), compared to the previous trapezoidal ( $S = 50$ ) unit cell. The goal of this design is to fix the narrow portions of the antenna arms (*right*), all  $4\mu\text{m}$  in width. The loss of periodicity also makes the design no longer invariantly scalable, the final design chosen and shown here has  $r_i = 29.8\mu\text{m}$ ,  $M = 6$ , and  $\tau = 1.35$ . (Color figure online)

## 3 Analysis

Various initial log-periodic designs were analyzed. The sinuous antenna was compared to that of [9], designed for the 95 and 150 GHz bands. It verified those results, yielding an oscillating arm impedance between  $\pm 40\%$  of the expected  $52.5\Omega$  and polarization wobble between  $\pm 5^\circ$ . The original/log-periodic trapezoidal showed minimally better polarization of  $\pm 4^\circ$  with larger impedance fluctuations of  $\pm 50\%$ . The first row of Table 1 outlines the initial sinuous design.

Antenna Design	$r_i$ ( $\mu\text{m}$ )	$M$	$\tau$	$L/R$	Beam Efficiency		Ellipticity (a-b)/(a+b)		Max. X-Pol
					150 GHz	220 GHz	150 GHz	220 GHz	
Sinuous	24	8	1.3	0.46	78.8%	–	0.04	–	2%
Bowtie	10	9	1.3	0.38	55.7%	45.4%	0.008	0.087	5%
Hybrid TZ.	29.8	6	1.35	0.42	85.5%	88.0%	0.017	0.045	2%

**Table 1** Parameters and simulated values for the initial sinuous design; along with bowtie and hybrid trapezoidal final designs.

### 3.1 Final Designs: Bowtie and Hybrid Trapezoidal

The hybrid trapezoidal design parameters were adjusted to best align impedance and polarization fluctuations with the final desired bands of 150 and 220 GHz. Inner radius  $r_i$  and expansion factor  $\tau$  shift and widen the impedance fluctuations, respectively. In that way, an impedance peak was fit between the desired bands, as shown *left* in Fig. 5. For most of both frequency bands, arm impedance is within  $20 - 40\Omega$ , reducing potential microstrip reflection although reactance fluctuations are a concern. The *right* image reveals the polarization wobble of each design, where the bowtie is better. Table 1 outlines the design parameters of each final antenna, along with beam efficiency and ellipticity at 150 and 220 GHz, calculated from directivity patterns. Parameter L/R refers to the ratio between the lens extension length and radius, which was optimized for marginally higher beam efficiency and directivity. The hybrid trapezoidal design showcases better beam efficiency (higher) and x-pol (lower) than the bowtie, while the ellipticity varies for both but stays below 0.1.

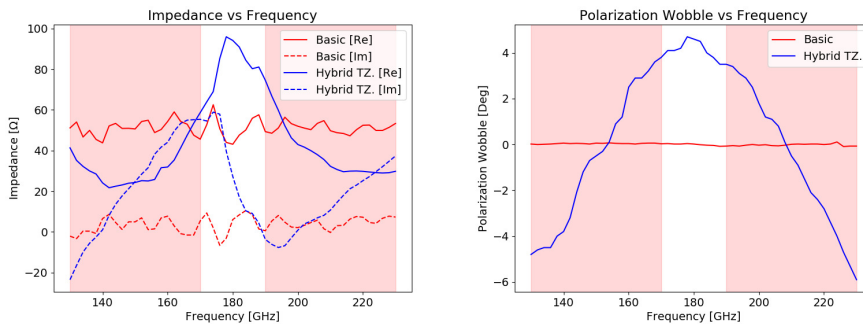


**Fig. 5** *Left*: Impedance of the final Bowtie and Hybrid Trapezoidal designs, with the Bowtie design close to the predicted  $52.5\Omega$  impedance. The Hybrid Trapezoidal stays between  $20 - 40\Omega$  resistance for the majority of the desired bands, but generates concern over impedance matching loss from the variable reactance. *Right*: Polarization Wobble, the Bowtie within  $\pm 0.2^\circ$  and Hybrid Trapezoidal  $\pm 5^\circ$ . (Color figures online)

## 4 Conclusion and Future Work

Both of the final antennas carry benefits. The bowtie offers accurate polarimetry for instances where beam efficiency is not a big concern, while the hybrid trapezoidal provides stronger detection with a wider polarization wobble. At lower frequency ( $< 40$  GHz) for which the CMB photon occupation number  $n_{occ} \gg 1$ , beam efficiency has a minimal impact on detector sensitivity. Then the much simpler bowtie antenna becomes the better choice.

Initial test arrays of the final designs have been fabricated. The arrays consist of antenna patterns on a silicon wafer, coupled via microstrip with multichroic Microwave Kinetic Inductance Detectors (MKIDs) which are multiplexed and read out from a single transmission line [11]. The AR-coated lenses are deposited onto the open silicon side, simplifying the array mount design. The next steps are to characterize their performance and update the designs for even larger arrays.

**Acknowledgements** This work is supported by NSF Grants AST-1509078 and AST-1711242 for Mauskopf; AST-1509211 and AST-1711160 for Johnson; AST-1506074 and AST-1710624 for Irwin. We would like to

acknowledge Dr. A. Suzuki (UC Berkeley) for his HFSS sinuous design, used in our initial comparison.

This is a post-peer-review, pre-copyedit version of an article published in Journal of Low Temperature Physics. The final authenticated version is available online at:  
<http://dx.doi.org/10.1007/s10909-020-02427-0>

## References

1. V. H. Rumsey, *Frequency Independent Antennas* (Academic Press, New York, 1966), DOI:10.1016/C2013-0-12216-7.
2. G. A. Deschamps, *IRE Trans. Antennas Propag.* **7**(5), 371 (1959), DOI:10.1109/TAP.1959.1144717.
3. O. Klemp, M. Schultz, and H. Eul, *Int. J. Electron. Commun. (AEU)* **59**(5), 268 (2005), DOI:10.1016/j.aeue.2005.05.007.
4. A. Suzuki, K. Arnold, J. Edwards, G. Engargiola, W. Holzapfel, B. Keating, A. T. Lee, X. F. Meng, M. J. Myers, R. O'Brient, E. Quealy, G. Rebeiz, P. L. Richards, D. Rosen, and P. Siritanasak, *J. Low Temp. Phys.* **176**, 650-656 (2014), DOI:10.1007/s10909-013-1049-5.
5. Planck Collaboration I, *A&A*, **594**, A1 (2016), DOI:10.1051/0004-6361/201527101.
6. W. Hu and M. White, *New Astron.* **2**, 323 (1997) DOI:10.1016/S1384-1076(97)00022-5.
7. R. O'Brient, PhD Thesis, University of California, Berkeley (2010).
8. J. M. Edwards, R. O'Brient, A. T. Lee, and G. M. Rebeiz, *IEEE Trans. Antennas Propag.* **60**, 4082 (2012), DOI:10.1109/TAP.2012.2207048.
9. A. Suzuki, PhD Thesis, University of California, Berkeley (2013).
10. O. Klemp, P. Damnoen, and H. Eul, *IEEE Antennas Propag. Society Int. Symposium*, 161 (2006), DOI:10.1109/APS.2006.1710478.
11. B. R. Johnson, D. Flanigan, M. H. Abitbol, P. A. R. Ade, S. Bryan, H.-M. Cho, R. Datta, P. Day, S. Doyle, K. Irwin, G. Jones, D. Li, P. Mauskopf, H. McCarrick, J. McMahon, A. Miller, G. Pisano, Y. Song, H. Surdi, and C. Tucker, *J. Low Temp. Phys.* **193**, 103 (2018), DOI:10.1007/s10909-018-2032-y.